Dynamic and Thermodynamic Examination of a Two-Stroke Internal Combustion Engine

Duygu İPCİ*, Halit KARABULUT[a]

[a]Gazi University Technology Faculty Automotive Engineering Department

(Geliş / Received : 27.06.2015 ; Kabul / Accepted : 24.07.2015)

ABSTRACT

In this study the combined dynamic and thermodynamic analysis of a two-stroke internal combustion engine was carried out. The variation of the heat, given to the working fluid during the heating process of the thermodynamic cycle, was modeled with the Gaussian function. The dynamic model of the piston driving mechanism was established by means of nine equations, five of them are motion equations and four of them are kinematic relations. Equations are solved by using a numerical method based on the Taylor series. By means of introducing practical specific values, the dynamic and thermodynamic behaviors of the engine were examined. Variations of several engine performance parameters with engine speed and charging pressure were examined. The brake thermal efficiency, cooling loss, friction loss and exhaust loss of the engine were predicted as about 37%, 28%, 4%, and 31% respectively for 3000 rpm engine speed and 1 bar charging pressure. Speed fluctuation was found to be 3% for 3000 rpm engine speed and 45 Nm torque.

Keywords: Two stroke engine, thermodynamic analysis, dynamic analysis, power and torque estimation, speed fluctuations.

ÖZ

Bu araştırmada iki zamanlı bir içten yanmalı motorun dinamik ve termodinamik birleşik analizi yapılmıştır. Termodinamik çevrimin yanma süresince çalışma akışkanına verilen ısının değişimi Gauss fonksiyonu ile modellenmiştir. Piston hareket mekanizmasının dinamik modeli dokuz denklemle modellenmiş olup bunlardan beşi hareket denklemi, dördü kinematik ilişkidir. Dinamik ve termodinamik modeli oluşturan denklemler Taylor serisine dayanan bir yöntemle çözülmüştür. Gerçekçi spesifik değerler kullanılmak suretiyle motorun dinamik ve termodinamik davranışları incelenmiştir. Muhtelif motor performans parametrelerinin motor hızı ve şarj basıncı ile değişimi incelenmiştir. 3000 rpm motor hızı ve 1 bar dolgu basıncı için termik fren verimi, soğutma kayıpları, sürtünme kayıpları ve egzoz kayıpları sırası ile %37, %28, %4 ve %31 olarak belirlenmiştir. 3000 rpm motor hızı ve 45 Nm tork için hız dalgalanmaları %3 olarak belirlenmiştir.

Anahtar Kelimeler: İki zamanlı motor, termodinamik analiz, dinamik analiz, güç ve tork tahmini, hız dalgalanmaları

1. INTRODUCTION

In piston engines the thermodynamic cycle is accomplished either by two or four reciprocating motions of the piston. The engines accomplishing a cycle by two reciprocating motions of the piston are named as two-stroke engines. The upward motion of the piston is a compression process while the downward motion is an expansion process. The discharge of burned gases and recharge of the fresh air, or air-fuel mixture, into the cylinder is performed towards the end of expansion process [1]. It is generally accepted that the two-stroke internal combustion engine was invented by Sir Dugold Clerk in Britain at the end of the 19th Century [1]. For the current situation the two-stroke internal combustion engines are used in a large variety of light and heavy duties.

In comparison with four stroke engines, the two-stroke engines have some advantages, such as simple structure, lower cost, lighter weight, higher specific power, higher speed, simple maintenance, capability of working at different positions, capability of being designed at very small scales and so on. It has also some disadvantages, such as relatively lower thermodynamic efficiency, higher HC and CO emissions as well as toxic pollutants [2-5], lower life time, specific lubricant requirement, wastage of some fuel through the exhaust port, specific crank case configuration requirement and so on. Both gasoline and Diesel fueled engines are able to be designed as a two-stroke engine [6].

Two-stroke engines are able to be designed with and without a valve mechanism. In engines having no valve mechanism, recharging of the fresh air into the cylinder and discharging of the exhaust gases out of the cylinder is accomplished by ports taking part on the cylinder wall. The opening and closing of the ports are performed by the piston motion [6]. The engines involving a valve mechanism are structurally complicated as four stroke engines but, via the valve mechanism, the rate of fresh air charged into the cylinder is increased as well as avoiding piston failures. In two-stroke engines, the work generation, discharging of the burned gases and recharging of the fresh air into the cylinder take part in the same stroke. Therefore, fresh air requires a pre-compression process into a pre-compression camber. Pre-compression may be performed by using a stepped-piston, a displacer, a blower, a pump or a compressor [6]. Beside these, the volume variation in the crankcase, due to the reciprocating motion of the piston, creates an adequate amount of pressure if the crankcase is properly

* *Sorumlu Yazar (Corresponding Author)*
e-posta:duyguipci@gazi.edu.tr
Digital Object Identifier (DOI) : 10.2339/2016.19.2 141-154

designed. In most of the two-stroke light-duty engines charging of the fresh air into the cylinder is performed by crankcase pressure. Obviously, in these types of engines the crankcase performs as a pre-compression chamber. In these engines, the flow of the fresh air into the crankcase may be performed by natural inspiration or by forced flow called as supercharging. Charging of fresh air into the cylinder via pre-compression process is an irreversible process and reduces the thermodynamic efficiency of the two-stroke engines except the case where the pre-compression is performed via a turbocharger. The two-stroke engines charged with crankcase pressure may have at most 1.5 times the power of four-stroke engines having the same cylinder volume if the flow of air into the crankcase is a natural inspiration. In the case of supercharging, the power of a two stroke engine approaches to a value of almost 2 times the power of four stroke engines.

The two-stroke engines charged with crankcase compression are simplest in structure. The crankcase compression is applicable only to the two-stroke gasoline engines. In these engines the exhaust port is located at somewhere before the bottom dead center of the cylinder. Discharging of exhaust gases starts when the upper piston ring coincides with the upper end of the exhaust port. Discharge of exhaust gases is a transient flow in the form of a pulse. Determination of discharging period of exhaust gases is a comprehensive fluid mechanic problem [7,8]. The intake port is located at somewhere a little lower than the exhaust port. After pulsing of exhaust gases, the intake port is disclosed by the piston top. For a certain time interval, both the exhaust port and intake port remains open. In terms of crankshaft angle, this period is called as scavenging angle [1]. The flow of fresh air from the crankcase to the cylinder is also a transient flow in the form of a pulse. In two-stroke engines the increase of the engine speed reduces the pulsing period of both exhaust gases and fresh air and reduces the efficiency of the charging. To address this problem, the high speed engines are designed with a larger crankcase compression ratio as well as designing ports that opens relatively earlier [1]. In two-stroke engines both of these design alterations have reducing effects on the engine thermal efficiency. In engines with moderate speeds, the statistical value of the crankcase compression ratio is about 1.4-1.5 [1]. In terms of the crank angle, the opening time of the exhaust port is about 50^{o}-70^{o} before the bottom dead center of the cylinder [1,6,9]. In two-stroke engines charged with crankcase compression, the flow of fresh air into the crankcase is performed through a piston controlled valve or a pressure controlled check-valve named as reed valve. In the engines with crankcase compression the crankcase cannot be used as a lubricant reservoir [10]. Therefore, the lubrication of sliding surfaces of the piston driving mechanism is performed via mixing some lubricant into the gasoline. The lubricant mixed into the gasoline reduces the octane number of the gasoline and, therefore, the compression ratio of the two-stroke engines is lower than that of four-stroke engines. The crankcase compression engines are not very useful for heavy duties. Heavy duty engines are mostly designed with pressurized lubrication and they use the crankcase as lubricant reservoir.

Some of the experimental investigations conducted in recent years on the internal combustion engines are concentrated on the heat release processes. According to the standard thermodynamic cycle of Otto engines, the total heat is given to the working fluid at the top dead center of the cylinder at a constant volume and the pressure of the working fluid increases a few times while the volume was constant. In practice however, this is a harmful phenomenon named as combustion knock. Combustion knock occurs in both Otto and Diesel engines. If the release of the heat is performed along a certain time interval, the knocking is avoided. Experimental investigations indicates that if the heat release period takes part in -5° and 25° of crankshaft angle around the top dead center, the combustion knock is avoided and the highest thermal efficiency is obtained [1,4,9,11,12]. The heat release interval of (-5°)-(+ 25°) is appropriate for both Otto and Diesel engines. As known, the cetane and octane numbers are criterions indicating knocking resistance of Diesel fuel and gasoline respectively. The compression ratio of the Otto engines is restricted to 11 by knocking.

Piston driving mechanism of the two-stroke engines is consisted of a piston, a connecting rod and a crankshaft. For the design of a pre-balanced crankshaft, a complete dynamic analysis of the piston driving mechanism is needed. In a dynamic analysis the gas pressure exerting onto the piston is an initially known function. The gas pressure may be obtained from an existing engine by measurement [13], or it may be determined by a thermodynamic analysis. The numerical data obtained by measurement is not useful to use in a dynamic analysis directly and require fitting with a Fourier series [13-15]. When it is fitted with a Fourier series, due to the nature of the Fourier series, the originality of the gas pressure is lost. Because of this the combined thermodynamic-dynamic analysis is seen more useful. In combined thermodynamic-dynamic analysis the gas force exerting onto the piston is calculated simultaneously with the other forces and moments involved by the analysis. For the calculation of gas force the first low of the thermodynamic given for closed systems is used [16].

A combined thermodynamic-dynamic analysis can be used for estimating the gas pressure, gas temperature, engine power, thermal efficiency, port timing values, speed-tork and speed-power characteristics of the engine, the transient and steady behaviors of the engine, mechanical design criterions such as strains, stresses, moments, forces and frictions, crankshaft speed fluctuations etc. The combined thermodynamic-dynamic analysis also enables the optimization of the

engine components from the weight or volume point of view.

In a dynamic system each component under force may have flexibility. Between sliding surfaces there may be working clearances as well. If the all of these flexibilities are taken into account, the degree of freedom of the dynamic model may become too large and too much time and effort is needed. To avoid this difficulty, dynamic analyses are restricted to examine the specific aspects of the dynamic systems. Similarly the components of piston driving mechanism and its different aspects are investigated by preparing specific dynamic models [17-20].

In four stroke engines having a valve mechanism, the friction losses are estimated as about 15% of indicated power [21,22]. In two-stroke engines, having no valve mechanism, the friction losses are significantly lower than that of four stroke engines [23]. In engines equipped with roll-bearings, the friction losses are further decreased. For two-stroke engines charged with crankcase compression, all of the friction losses are estimated to be (5-10)% of the indicated work.

In two-stroke engines charged with crankcase compression the highest frictional loss appears at the piston-cylinder liner interface. The total friction force exerted on a piston is mainly caused by skirt friction and ring-pack friction. The piston skirt and ring-pack comprise both hydrodynamic and boundary frictions (asperity friction). The simplest approximation used for calculating the hydrodynamic friction between piston skirt and liner is the Couette approximation. Ring-pack friction depends on many physical factors such as gas pressure, secondary motion of the piston, static and dynamic distortions on the cylinder bore, starvation of the lubricant around the ring contact surface, the non-axisymmetrical form of rings in the cylinder bore and so on[24-27]. About the top and bottom dead centers of the piston stroke, the tilting motion of the piston causes a higher asperity friction. At mid regions of the piston stroke, the hydrodynamic friction is dominant. The experimental measurement conducted without the working gas pressure indicates that the sum of asperity friction and hydrodynamic friction could be accepted as constant [18,26].

In two-stroke engines charged by the crankcase compression, the connection of the crankshaft with the conrod and the engine body, or the crankcase, is made with roll bearings. In very small engines the ball type, in relatively large engines needle type roll bearings are used. To calculate the roll bearing friction, 5 different approximation models were developed, such as rotary coulomb friction model, bearing/seal viscous model, Palmgren model, ATEC bearing model and SKF bearing model [28]. However these are not the only approximations found in the whole of the roll bearing literature. In a roll bearing sources of the friction are: elastic hysteresis in rolling, sliding due to deformation of contacting elements and/or bearing geometry, spinning of rolling elements, gyroscopic pivotal motion of rolling elements, sliding between cage and rolling elements and between cage and bearing rings, viscous friction due to lubricant motion and seal friction. The hydrodynamic friction is related to the speed of the shaft and in some cases it may become 98% of the total friction. The variation of the other components of friction with speed may be negligible [29]. The friction caused by sliding due to deformation of contacting elements and/or bearing geometry has a strong dependency on normal forces [30,31].

In most of the theoretical studies related to the piston driving mechanism dynamic, conducted so far, the conrod mass is divided into two parts and one of them is added to the piston as the other is added to the crankshaft mass [26,32,33,34]. There are also a few numbers of studies treating the conrod as a separate part of the dynamic system [35]. In these studies the conrod motion was described by three equations which are translational x and y momentum equations and angular momentum equation around the gudgeon pin. This model provides more precise prediction of the mass of counter balance weights and their positions.

One of the important aspects of the thermodynamic-dynamic analysis is the inclusion of heat transfer between the working gas and cylinder walls. The largest amount of the heat transfer occurs around the combustion chamber. The determination of the heat transfer coefficient in the engine cylinders is a comprehensive study field including theoretical and experimental analysis. The correlation given by Eichelberg and Nusselt are most recommended approximation for engine heat transfer calculations [16,36].

This analysis is intended to estimate the thermodynamic performance characteristics and the optimization of mechanical quantities of a two-stroke gasoline engine charged with crankcase compression. The dynamic model has one degree of freedom and involves 5 motion equations as well as kinematic relations. The present analysis involves three different novelties. In some of previous analysis the gas pressure was obtained from an empirical relation which is Fourier expansion of experimental data obtained from a test engine. Also, some of previous analysis uses theoretical data generated from standard ideal gas cycles. In the present analysis the gas pressure have been obtained from a relation derived from the first law of the thermodynamic which involves the heat release rate and heat transfer to the surrounding walls. Another novelty is the use of a heat release rate profile to provide heat for the thermodynamic cycle involved by the present analysis. The heat release rate profile used in the analysis has been established by means of resembling the experimental heat release rate profiles presented in some latest experimental works [3,4]. The third novelty is that in the present analysis the conrod motion was modeled by means of three motion equations differently from previous analysis where the conrod was split into

two parts and parts were added to crankpin and piston masses. The analysis presented here will enable the design of pre-balanced crankshafts.

2. MATHEMATICAL MODEL

Figure 1 illustrates mechanism and some of nomenclature used in the analysis. The crankshaft center is the center of the general coordinate system. The initial position of the mechanism corresponds to $\theta = 0$. For angular displacements and moments, the anticlockwise direction was assumed to be positive. For the situation seen in Figure 1, both the crankshaft and conrod rotates in anticlockwise direction. All of the components are assumed to be rigid. Secondary motions caused by working clearances are disregarded. Equations are derived by Newton method.

Regarding the conrod force, hydrodynamic friction, the piston skirt load-dependent friction and piston ring pack frictions exerting on the side surface of the piston and gas forces exerting on the top and bottom surfaces of the piston, the motion equation in y coordinate may be written as

$$F_{by} = \begin{pmatrix} m_p \dfrac{d^2 y_p}{dt^2} + F_w - F_{ch} + C_p \dot{y}_p + \\ F_\infty sgn(\dot{y}_p) + C_s F_{bx} sgn\left(\dot{y}_p\right) \end{pmatrix} \quad (1)$$

where the ring pack and skirt asperity frictions are indicated by the terms $F_\infty sgn(\dot{y}_p)$ and $C_s F_{bx} sgn\left(\dot{y}_p\right)$ respectively [30].

The mass center of the conrod displays a two dimensional motion. Except this, the conrod displays a rotational motion around the gudgeon pin as well. The complete motion of the conrod can be described by translational equations of motion in x and y coordinates and the angular equation of motion around the gudgeon pin. The translational motion equations in x and y coordinates are

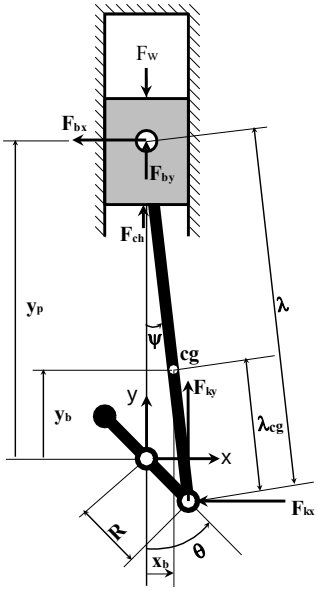

Figure 1. Mechanism, coordinates and nomenclature

$$F_{bx} = m_b \frac{d^2 x_b}{dt^2} + F_{kx} \quad (2)$$

$$F_{ky} = m_b \frac{d^2 y_b}{dt^2} + F_{by} . \quad (3)$$

The big and small ends of the conrod are connected to the crankpin and gudgeon pin. The friction at the gudgeon pin can be disregarded. However, the friction at the big end bearing may be significant. By regarding forces exerted by the crank pin and the moments generated by the bearing hydrodynamic and load-dependent frictions, the angular motion equation of the conrod is derived as

$$F_{kx} = \frac{-I_b \dfrac{d^2\psi}{dt^2} + F_{ky}\lambda \sin\psi + C_{km}\left(\dot{\theta} - \dot{\psi}\right) + M_f}{\lambda \cos\psi} \quad (4)$$

where M_f indicates the load-dependent components of the roll bearing frictions. At low speeds M_f varies a bit with speed but, its variation terminates after a certain value of speed and becomes stable [31]. The sum of components of the roll bearing frictions except the hydrodynamic component may be calculated by the SKF model. The load exerting on the conrod roll bearing should be the resultant of F_{ky} and F_{kx} which are seen in Figure 1. In this analysis the SKF needle bearing numbered with NK 35/30 was found to be appropriate for the crank pin and main journals of the two-stroke engine having 80 mm piston diameter. By substituting the all specific values of the needle bearing of NK 35/30 into the SKF model [37], the frictional tork of the crankpin needle bearing was stated as

$$M_f = 0.5 \times 0.0022 \times 0.035 \sqrt{F_{ky}^2 + F_{kx}^2} . \quad (5)$$

By regarding conrod forces, the frictional moment in conrod big end bearing, the frictional moment in the main journal bearing, starter moment and the external moment applied by the foundation, the crankshaft motion equation was derived as

$$\frac{d^2\theta}{dt^2} = \frac{\begin{pmatrix} M_s - M_q - F_{ky} R \sin\theta + F_{kx} R \cos\theta - \\ C_{km}\left(\dot{\theta} - \dot{\psi}\right) - C_h \dot{\theta} - M_f - M_\tau \end{pmatrix}}{I_{kr}} \quad (6)$$

where M_s and M_q are taken as constant values. M_τ is in the same category with M_f [31] and can also be calculated by SKF model . If the same needle bearing identified above is used, the friction moment becomes

$$M_\tau = 0.5 \times 0.0022 \times 0.035 \sqrt{\frac{F_{ky}^2}{4} + \frac{F_{kx}^2}{4}} \quad (7)$$

In Equation (6), C_{km} and C_h, are hydrodynamic friction coefficients with constant values. The values of

C_{km} and C_h can be determined by using the SKF friction model as well.

The kinematic relations used for the calculation of; the angle between the conrod and cylinder axis, the vertical distance between the crank center and piston top, the vertical distance between the crank center and the conrod mass center and the horizontal distance between the crank center and conrod mass center are

$$\psi = \arcsin\left[\frac{R}{\lambda}\sin\theta\right] \tag{8}$$

$$y_p = -R\cos\theta + \lambda\cos\psi + h_p \tag{9}$$

$$y_b = -R\cos\theta + \lambda_{cg}\cos\psi \tag{10}$$

$$x_b = (\lambda - \lambda_{cg})\sin\psi\,. \tag{11}$$

For the calculation of the in-cylinder pressure, an equation was derived from the first law of the thermodynamic. For the systems with constant mass, the first law of the thermodynamic is given as

$$dq = du + pdv\,. \tag{12}$$

The perfect gas law is given as

$$dT = \frac{1}{\Re}d(pv)\,. \tag{13}$$

Equation (12) may be rearranged as

$$\frac{dq}{T} = \frac{\Re}{k-1}\frac{dp}{p} + \left[\frac{\Re k}{k-1}\right]\frac{dv}{v}\,. \tag{14}$$

In last equation q indicates the net heat calculated as $q = q_p - q_w$, where q_p is the heat generated by the combustion and q_w is the heat loss via the heat transfer between the gas and walls surrounding the gas. Equation (14) can be arranged as

$$\frac{dp}{p} + k\frac{dv}{v} = (k-1)\frac{d(q_p - q_w)}{pv}\,. \tag{15}$$

When the last equation is integrated between two thermodynamic states of the gas, $i-1$ and i

$$p_i = \frac{p_{i-1}v_{i-1}^k}{v_i^k}e^{\left[(k-1)\int_1^2\frac{dq_p}{p_iv_i} - (k-1)\int_1^2\frac{dq_w}{p_iv_i}\right]} \tag{16}$$

is obtained. The last equation can be rearranged as below, by assuming that the gas in the cylinder is not 1 kg and, between states $i-1$ and i, its thermodynamic values change at a differential order,

$$p_i = \frac{p_{i-1}V_{i-1}^k}{V_i^k}e^{\left[\frac{k-1}{p_iV_i}\Delta Q_p - \frac{k-1}{p_iV_i}\Delta Q_w\right]}\,. \tag{17}$$

Via the cooling law of Newton, last equation can be rearranged as

$$p_i = \frac{p_{i-1}V_{i-1}^k}{V_i^k}e^{\left[\frac{k-1}{p_iV_i}\Delta Q_p - (k-1)\,hA_i\left(\frac{1}{m\Re} - \frac{T_w}{p_iV_i}\right)dt\right]} \tag{18}$$

In the last equation if p_i on the right is replaced with p_{i-1}, the equation transforms to a more useful form. The error caused by this perturbation is too small to influence the accuracy of the pressure.

In this study, the heat produced during a differential rotation of the engine was correlated with Gauss function as

$$\Delta Q_P = C\cdot e^{-\Omega[\theta-\varphi-(n-1)2\pi]^2}\omega\Delta t\,. \tag{19}$$

In this equation φ, Ω and C are constants qualifying the location of maximum heat production, the duration of heat production and the amount of heat production. n is an integer indicating the number of strokes. If the last equation is integrated over a cyclic period, the relation: $C = (Q_P\,\Omega^2)/\pi$ is obtained which indicates that C and Ω are interrelated.

For the calculation of heat transferred from the gas to the wall, the Eichelberg and Nusselt relations

$$h = \frac{77.9\sqrt{pT}}{10000}\;V_P\,, \tag{20}$$

$$h = 5{,}388\times10^{-4}(1+1{,}24V_p)T^{1/3}p^{2/3} + 0{,}421\left[\frac{\left(\frac{T}{100}\right)^4 - \left(\frac{T_w}{100}\right)^4}{T - T_w}\right] \tag{21}$$

were used [16,36]. In these equations V_P is the average speed of the piston and initially not known. In last two equations if V_P is replaced with $0.64R\dot{\theta}$, equations becomes more eligible to use in a simulation program.

Due to the high speed motion of crankshaft and other components, the air in the crankcase has a large enough circulation velocity. Because of this velocity, the heat transfer coefficient between the crankcase wall and the air is large enough. Therefore the pre-compression in the crankcase may be assumed as an isothermal process. Regarding this situation the pressure in the crankcase may be defined by a piecewise function as

$$p_i = \begin{cases} 10^5, & 0 \le \theta \le \pi \\ \dfrac{p_{i-1}V_{i-1}}{V_i} & \pi \le \theta \le 2\pi \end{cases} \tag{22}$$

If the opening and closing times of the intake and exhaust ports are taken into account, the last equation is not a precise definition of the crankcase pressure however; for the sake of simplicity of simulation program, the last equation is preferred.

If the forces exerting on the engine body are minimized, the vibration of the engine body is minimized. The

resultant of forces exerting on engine body may be determined via setting static balance equations in y and x directions. The external forces exerting on the engine body are the external support forces, gas forces in crankcase and working volumes, friction forces inside the engine block and forces conducted to the engine block via the crankshaft and piston contact surfaces. The static balance equations of the engine body in y and x direction may be written as

$$F_{zy} + F_w - F_{ch} - C_p \dot{y}_p - F_\infty sgn(\dot{y}_p) - C_s F_{bx} sgn\left(\dot{y}_p\right) - F_{ky} = 0 \quad (23)$$

$$F_{zx} + F_{kx} - F_{bx} = 0 . \quad (24)$$

By combining Equations (23),(3) and (1)

$$F_{zy} = m_b \frac{d^2 y_b}{dt^2} + m_p \frac{d^2 y_p}{dt^2} \quad (25)$$

is obtained. By combining Equations (24) and (2)

$$F_{zx} = m_b \frac{d^2 x_b}{dt^2} \quad (26)$$

is obtained. Last two equations indicate that, the resultant forces exerting on the engine body are inertia forces only. The forces described by the last two equations work to vibrate the engine block. In order to balance these forces, counter weights are used. A counterweight generates a centrifugal force in the positive radial direction. If the counter weight is situated opposite to the crank pin, the centrifugal force generated by the counterweight balances the force generated by piston and conrod. The vertical and horizontal components of the centrifugal force generated by counter weight may be defined as

$$F_{dy} = m_d \dot{\theta}^2 R_d \cos\theta \quad (27)$$

$$F_{dx} = m_d \dot{\theta}^2 R_d \sin\theta \quad (28)$$

where m_d and R_d are the mass and radial distance of the counter weight. From the numerical solution point of view, equations derived above are an initial value problem. The boundary conditions of crankshaft angle and gas pressure are

$$t = 0, \quad \theta = 0, \quad \dot{\theta} = 0 \quad (29)$$

$$t = 0, \quad p = 1 \ bar . \quad (30)$$

The boundary conditions of the other variables are derived easily from the kinematic and dynamic relations given above. Numerical solution of equations is performed by a method based on Taylor series expansion [15,32]. The solution of the dynamic model is progressed as same as the operation of an internal combustion engine. At first, the crankshaft is accelerated by the starter moment and the whole of the dynamic system gains momentum. Up to a certain value of the crankshaft angle the starter moment is kept active and the system is let to perform the first expansion process. After the expansion process, system gains adequate momentum and keeps running.

3. RESULTS AND DISCUSSION

Specific values used in the analysis are listed in table 1. Figure 2 illustrates the angular distribution of the heat released per degree of crankshaft angle. The angular distribution of the released heat was presented by Gaussian function where the peak of the Gaussian distribution corresponds to 192°. The total of the released heat per cycle is 779.87 J; and 729.78 J of this heat is released within the angles of 177°-207°. Respect to this distribution, 93.6% of the released heat is performed within a 30° of crankshaft angle around 192° where 192° may be named as the midpoint of heat release interval. At stoichiometry conditions the heat released should be 894 J. However, in modern internal combustion engines the use of 100% fresh air is avoided because that in the case of using 100% fresh air the NO_x level in the exhaust gases exceeds limitations forced by some national and international legislations. To satisfy legislations, fresh air is mixed with some exhaust gas such as 5% - 15%. In this study the exhaust gas ratio mixed into the fresh air is assumed to be about 13%. On the other hand, in two-stroke engines inherently some exhaust gas mixes into the fresh air due to the scavenging of intake and exhaust ports. Regarding this situations the heat release per cycle is determined as 779.87 J. The heat release profile given in Figure 2 is very consistent with ones given in references [3,4] which are experimental findings.

Table 1. Specific values used in the analysis

Diameter of the piston	0.08 m
Location of midpoint of heat release interval (φ)	192°
A dimensionless constant to quantify the released heat (C)	2200
A dimensionless constant to quantify the heat release duration (Ω)	-25
Length of the conrod (λ)	0.16 m
Distance from conrod big end center to gravity center (λ_{cg})	0.04 m
Crank radius (R)	0.04 m
Crankcase inlet pressure (p_∞)	10^5 bar
Mass of piston (m_p)	0.6 kg if different, is given in the text
Mass of conrod (m_b)	0.4 kg if different, is given in the text
Torsional viscous damping coefficient at conrod bearing (C_{km})	0.002 N m s/rad

Torsional viscous damping coefficient at main bearing (C_h)	0.006 N m s/rad
Dimensionless friction coefficient at piston side surface (C_s)	0.05
Lateral viscous damping coefficient at piston side surface (C_p)	2.0 N s/m
Ring pack friction (F_∞)	20 N
Gas constant of air $(\Re)$	288.0 J $kg^{-1}K^{-1}$
Specific heat at constant pressure/Specific heat at constant volume (k)	1.35
Inlet temperature of the fresh air into the cylinder (T_{in})	350 K
Average wall temperature of cylinder (T_w)	400 K
Lower heating value of fuel	42000 kJ
Distance between piston top and gudgeon pin center (h_p)	0.05 m
Volume of crankcase corresponding to $\theta = 0$	10^{-3} m^3
Volume of combustion chamber	$44x10^{-3}$ m^3
Crankshaft mass inertia moment (I_{kr})	0.0567 m^2kg
Conrod mass inertia moment (I_b)	0.0025 m^2kg
Radial distance of counter weight from the crankshaft center (R_d)	0.05 m
Starter motor moment (M_s)	60 Nm

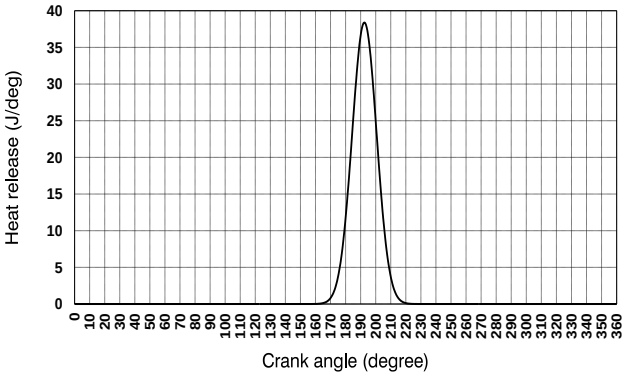

Figure 2. Heat releases during a cycle.

In a thermodynamic-dynamic analysis, the highest error may be imposed by the used heat transfer relations. In this analysis the heat transfer from gas to the wall was calculated via two relations given by Nusselt and Eichelberg. Figure 3 illustrates cumulative of the heat release, the indicated work generation, the cooling loss (heat transfer to the walls) and the exhaust loss over a period of 43 cycles. Data used in Figure 3 were obtained by using Nusselt relation in the simulation program [16,36]. As seen from the figure the cumulative heat release, the indicated work generation, the cooling loss and the exhaust loss are varying linearly with time. In each of subsequent cycles, an equal amount of heat release, work generation, cooling loss and exhaust loss are observed. This is due to that all of these quantities are not varying from cycle to cycle. The curve indicating the heat release increases step by step like stairs. This is due to that in a cyclic period, the heat release occurs within a 50^o of crank angle and in the remaining of the cycle the heat release is zero.

Data used in Figure 3 for cooling loss, indicated work and heat release were determined directly by the analysis. The exhaust loss was calculated by balancing the cooling loss, the indicated work and the heat release. The heat release, the cooling loss, the work generation and the exhaust loss over a period of 43 cycle are 33536.27, 9622.62, 13731.66 and 10182 J respectively. According to these results, 40.94% of the released heat is converted to the work, 28.69% is transferred to the wall and 30.36% is lost through the exhaust. These proportions are consistent with practical measurements.

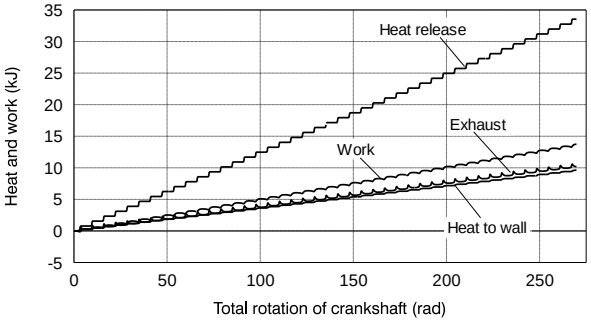

Figure 3. Comparison of the heat release, indicated work, cooling loss and exhaust loss

In simulation program if the Eichelberg relation is used instead of Nusselt relation, the results presented in Figure 4 were obtained. The heat released during 41 cycles is 31977 J. The cooling loss, the work generation and the exhaust loss are 18246, 9369.02 and 4361 J respectively. According to these results, 29.3% of the released heat is converted to the work. 57.05% is transferred to the wall. 13.63% is taken away by the exhaust gases. These proportions are inconsistent with practical measurements. As the result, the heat transfer relation given by Eichelberg was found to be not appropriate to use in this analysis. The numerical result used in the remaining of this analysis was obtained by the Nusselt relation.

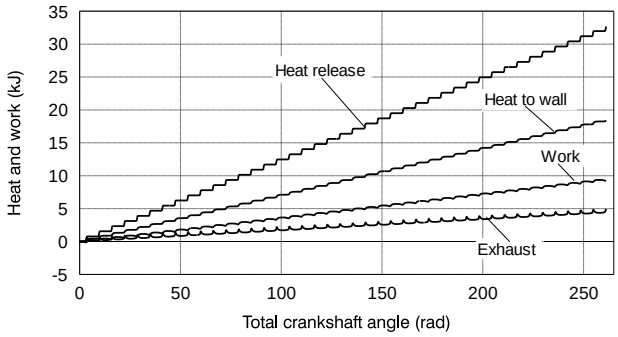

Figure 4. Comparison of the heat release, indicated work, cooling los and exhaust losses[16,36].

Table 2 indicates variations of indicated efficiency, proportion of friction losses to the indicated work, shaft work, indicated work, engine torque, crankshaft speed and thermal efficiency versus the location of midpoint of heat release interval. The results presented in Table 2 are obtained for the constant speeds of 313 rad/s. As seen in Table 2, the maximum values of indicated efficiency, shaft work, indicate work, engine torque and brake thermal efficiency appear for midpoint of 192^o. This value of midpoint is consistent with experimental findings [4]. Particularly the brake thermal efficiency obtained from this analysis is very consistent with experimental findings given for two-stroke engines [9]. On the whole, the position of the midpoint causes no drastic variations in the examined interval.

Results given in Table 2 were obtained by disregarding the pumping losses of fresh air. If the compression of fresh air in the crankcase is assumed to be isothermal and the pumping loss is included in the simulation program, the results seen in table 3 are obtained. When table 2 and 3 are compared, it is seen that indicated works are the same. Shaft work in table 3 is lower than the shaft work in table 2. The deviation is caused by pumping losses. As the result of this deviation, the overall brake efficiency of the engine declines 1% more down. In reference [9], the brake thermal efficiency of a two- stroke diesel engine fuelled with alcohol is given as about 33% which is very consistent with the findings of this analysis. According to the Table 3, the energy distribution between shaft work, cooling heat, friction and pumping losses, and exhaust losses was determined as about 37%, 28.3%, 4.1%, and 30.6% respectively.

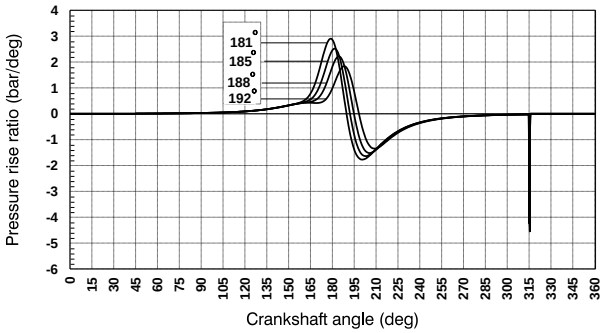

Figure 5. Variation of the pressure rise ratio with the location of midpoint of heat release interval

In Figure 5 the pressure rise ratio per degree of crankshaft angle was illustrated versus the crankshaft angle and midpoint of heat release interval. In the design of internal combustion engines the pressure rise ratio is a very important criterion. In the case of that the pressure rise ratio exceeds a certain value, the engine knock phenomenon occurs. In the literature of internal combustion engines the critical value of the pressure rise ratio was presented as $\frac{dp}{d\theta} = 10\, bar/\deg$ [39,40,41]. According to the Figure 5, the pressure rise ratio is far enough from the knocking condition.

Figure 6 illustrates comparison of in-cylinder pressure profiles of cycles: polytrophic with heat release and heat transfer, polytrophic with heat transfer but no heat release and completely adiabatic. The pressure of the adiabatic cycle should be lower than that of polytrophic cycle with heat release and heat transfer but, should be higher than that of polytrophic cycle without heat

Table 2. Variation of the thermodynamic performance parameters with the midpoint angle of heat release interval

ψ (deg. of CA)	η_i (%)	W_f / W_i (%)	W_b (J/cyc)	W_i (J/cyc)	M_b (Nm)	ω (Rad/s)	η_b (%)
181	39.65	8.59	282.74	309.33	45	313.07	36.24
185	40.62	8.39	290.28	316.88	46.2	313.02	37.21
188	41.01	8.14	293.73	319.77	46.75	313.03	37.67
192	41.07	8.20	294.05	320.34	46.80	313.08	37.70
195	40.81	8.22	292.16	318.37	46.5	313.10	37.45
198	40.34	8.36	288.39	314.70	45.9	313.09	36.97

Table 3. Thermodynamic parameters obtained for 192^o of midpoint by regarding pumping losses

ψ (deg. of CA)	η_i (%)	$\left(W_f + W_p\right) / W_i$ (%)	W_b (J/cyc)	W_i (J/cyc)	M_b (Nm)	ω (Rad/s)	η_b (%)	Q_c (J/cyc)
192	41	10	288.7	320	45.95	313.2	37	221

release. As seen from Figure 6, profiles are consistent with expectations. The difference between the adiabatic curve and polytrophic curve with heat transfer is an indication of the rate of heat transfer to the wall.

The pressure profile of the polytrophic cycle with heat release and heat transfer was obtained using the heat-release profile seen in Figure 2 where the midpoint is 192^o of crank angle. The ratio of the peak pressure of the polytrophic cycle to the other peak values is 2.022 and 1.85. These values are very consistent with practical results [9]. The peak value of the gas pressure of the polytrophic cycle with heat release and heat transfer appears at 198^o of crankshaft angle.

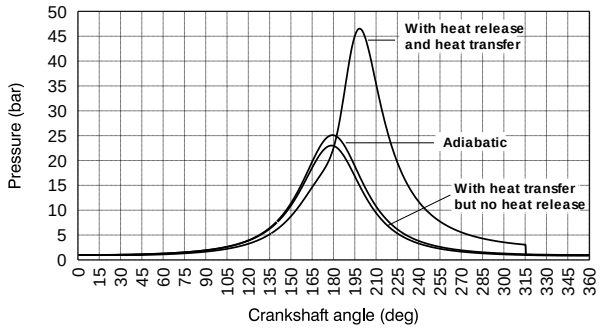

Figure 6. Comparison of pressure profiles obtained for polytrophic cycle with heat release and heat transfer, polytrophic cycle with heat transfer but no heat release and adiabatic cycle.

Figure 7 illustrates the temperature profile of the working gas of the engine comparatively with that of adiabatic and polytrophic cycles having no heat release. The temperature of the fresh air was assumed to be 350 K. The temperature profile of the engine was obtained for the heat release depicted in Figure 2. During the heat release period the increase of the temperature is about 2.73 times the after-compression temperature of gas. The exhaust gas temperature of the engine before the pulsation is 1265 K or 992^oC which is very consistent with practical findings [3]. According to Figure 6, when the exhaust port is on the position of disclosing, the pressure of the gas is 3.06 bars. By assuming that the pulsation of the exhaust gases is an isentropic process, the after pulsation temperature of the exhaust gas was calculated as 919.73 K or 646.73 ^oC.

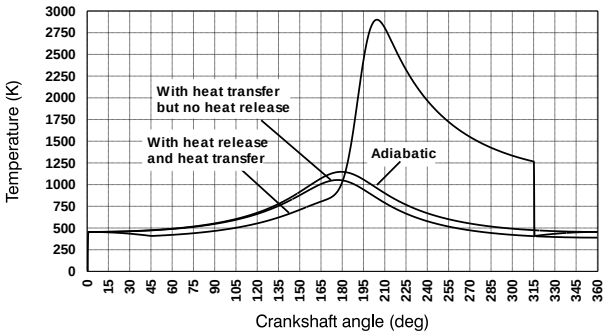

Figure 7. Variation of the gas temperature during a cycle

Figure 8 illustrates the P-V diagram of the engine. The effective compression ratio is determined as 9.037. The appearance of the P-V diagram is consistent with practical Otto cycle. In this engine 25% of piston stroke is devoted to discharging and recharging of the working fluid. As seen from Figure 8, the work loss due to this period is not very significant.

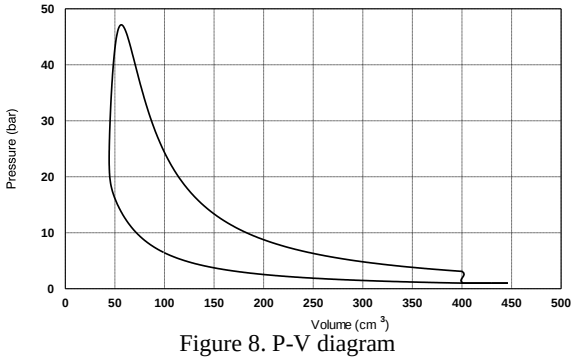

Figure 8. P-V diagram

In Table 4 and Figure 9, thermodynamic values

Table 4. Thermodynamic values obtained from the analysis for $\lambda = 1.146$, $\dot{\theta} = 313\ rad/s$, $\varphi = 192^\circ$ and $0.5 \le p_\infty \le 1\ bar$

Crankcase pressure (bar)	η_i (%)	η_b (%)	W_b (J/cyc)	W_i(J/cyc)	$\frac{W_f+W_p}{W_i}$ (%)	M_b (Nm)	Q_p (J/cyc)	$Q_{\lambda=1}$(J/cyc)
1.0	41.08	36.73	286.51	320.45	10.59	45.6	779.91	893.83
0.9	40.73	36.26	254.47	285.83	10.97	40.5	701.62	804.45
0.8	40. 39	35.56	221.79	251.88	11.95	35.3	623.62	715.07
0.7	39.99	34.71	189.44	218.26	13.20	30.15	545.74	625.68
0.6	39.49	33.58	157.08	184.72	14.96	25.0	467.75	536.3
0.5	38.93	31.99	124.72	151.79	17.83	19.85	389.86	446.91

obtained for $\lambda = 1.146$, $\dot{\theta} = 313\ rad/s$, $\varphi = 192^{\circ}$ and $0.5 \le p_{\infty} \le 1\ bar$ were presented. This examination corresponds to a constant speed testing of the engine. In experimental investigations the air used by the engine is quantified by the throttle valve position. In this study instead of throttle valve position, the crankcase inlet pressure has been used. As seen in Figure 9, while the crankcase inlet pressure decreases, the brake torque, heat input and indicated work decreases linearly. Indicated thermal efficiency and brake thermal efficiency displays accelerating decreases but, until 0.5 bar, the decrease of thermal efficiencies is not a drastic variation. From practical point of view, this is an advantageous aspect of this engine. The ratio of $(friction\ loss + pumping\ loss)/indicated\ work$ displays an accelerating increase. Acceleration of $(friction\ loss + pumping\ loss)/indicated\ work$ is caused by that both the nominator and denominator of the fraction decreases but the decrease of the denominator is larger than the decrease of nominator. At full throttle the engine analyzed here seems to be able to generate 14.27 kW power. The specific power of the engine per liter will be about 32 kW.

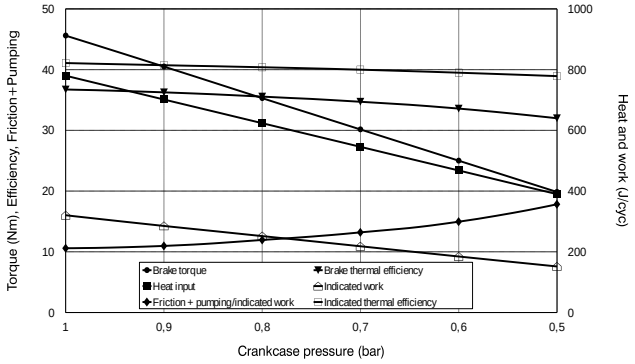

Figure 9. Variation of torque, thermal efficiencies, heat input, indicated work and ratio of losses to indicated work

Figure 10 illustrates a speed profile obtained from a case study. The engine is put in motion via a starter having 60 Nm torque. Before the starter begins to rotate the engine, the piston is at the bottom dead center. If the starter moment is applied during an initial motion of 7 radians, then the engine gains adequate momentum and continues to run by its own. Within the first two revolution of the crankshaft, via the starter moment, the crankshaft speed displays a rapid increase. Until the crankshaft rotates 100 radians, the external moment (load) is not applied. During this period, the crankshaft displays a decelerating increase. The deceleration is caused by the friction which is increasing with speed. After 100 radians, a critical external moment is applied so as to keep the average speed of the engine constant. The critical value of the external moment was obtained by trial and error. Over the stable running domain beyond 100 radians, the average speed of the crankshaft, corresponding to a 45 Nm critical torque, is 416 rad/s. The maximum and minimum values of the speed are 421.12 and 410.91 rad/s. The ratio of fluctuation to average speed is 2.40%. In four-stroke engines having a similar crankshaft mass-inertia-moment, the speed fluctuation is more than two times the calculated value here [13,32]. Lower fluctuation is an advantage of the two-stroke engines. The kinetic energy variation of the crankshaft caused by speed fluctuation is roughly 290 J.

The exaggerated view appended to Figure 10 shows the cyclic variation of the crankshaft speed at steady stead running conditions. The period $0 \le \theta \le \pi$ is a compression process. The second part, $\pi \le \theta \le 2\pi$, is an expansion process. During the first part, the net energy transferred to the reciprocating elements is zero because of that the initial and final speeds of the reciprocating elements are the same. During the first part, the decrease of crankshaft speed is about 10 radians. The kinetic energy variation of the crankshaft is about 241 J. The energy transferred from the crankshaft to the gas and foundation is about 141 J. The difference between these two values is frictional losses and compression work.

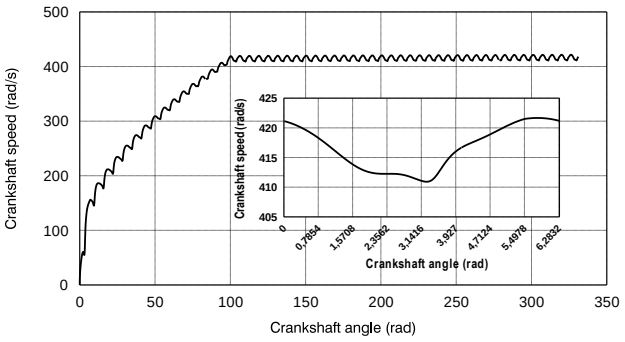

Figure 10. Crankshaft speed fluctuations

Figure 11 illustrates variation of the crankshaft speed with external load. In practice this operation is called speed testing. All of the speed profiles seen in Figure 11 were obtained at 100% throttle openness. While the speed increases, the external load applicable to the engine decreases. This is caused by the increase of frictional losses. In practical speed testing of real engines, the decrease of the torque is caused mainly by two factors such as natural throttling of the intake air due to viscous flow losses and frictional losses of the engine. This analysis does not involve natural throttling of the intake air. Therefore the speed profiles obtained here differs from the practical ones. In real engines, after a certain value of crankshaft speed, engine tork may decline. As seen from Figure 11, while the mean speed increases, the fluctuation decreases. The relation between the mean speed and fluctuation seems to be linear. While the mean speed increases the brake torque displays a decelerating decrease.

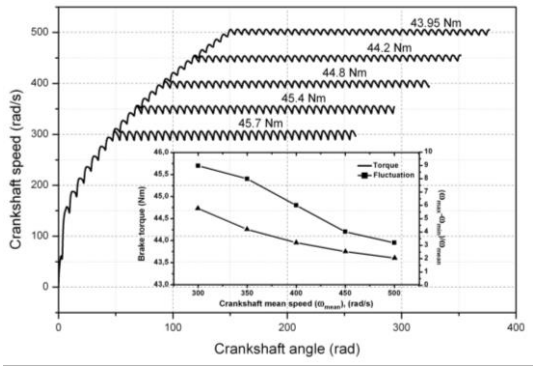

Figure 11. Variation of crankshaft speed with external load

Figure 12 illustrates vertical components of the piston and conrod force and the counter weight force obtained from a case study. The case study was conducted for 4000 rpm engine speed. In this case study, both the piston and conrod masses were taken to be 500 g and the mass of the counter weight was predicted as 600 g. The crankshaft used here is assumed to be statically pre-balanced without conrod and piston. As seen from Figure 12, peak values of vertical force generated by the piston and conrod is about 4265 N. The peak value of the vertical force generated by a counter weight is about 2766N. The difference of vertical forces generated by piston and conrod, and counter weight is 1500 N. So, the vertical unbalance is reduced from 4265N to 1500N.

Figure 13 illustrates horizontal components of the piston and conrod force and the counter weight force obtained from the same case study mentioned in Figure 12. As seen from Figure 13, peak values of vertical force generated by the piston and conrod is about 1500 N. The peak value of the vertical force generated by a counter weight is about 3000 N. The difference of horizontal forces generated by piston and conrod, and counter weight is 1500 N. So, the horizontal unbalance is not reduced. The counter weight has no reducing effect on the horizontal unbalance. On the contrary, the counter weight increases the horizontal unbalance as much as that it reduces the vertical unbalance. In some applications the vertical unbalance may be harmless; in such a case counter weight may be completely unnecessary, or vice versa. From this case study we observe that the mass of the piston and conrod should be as small as possible.

Figure 14 illustrates comparison of the counter weights obtained from the present study and former studies. In former analysis the conrod mass was split into two parts as $30m_b/100$ and $70m_b/100$. The part $30m_b/100$ was added to the piston mass while the other was added to the crankshaft mass. The static balancing of the crankshaft is thought to be performed after addition of the part $70m_b/100$. Therefore, in previous studies, the unbalance struggling to vibrate the engine is generated by the piston mass and 30% of the conrod mass. According to the previous studies the mass of the counter weight may be predicted via the correlation,

$$m_d = 0.5\frac{R}{R_d}\left(m_p + \frac{30}{100}m_b\right) \tag{31}$$

which was obtained by correlating numerical results [32]. Into this correlation, by substituting $m_p = 0,5\,kg$, $m_b = 0,5\,kg$, $R = 0,04\,m$ and $R_d = 0.05\,m$, the mass of counter weight is predicted as 0.26 kg. In Figure 14A the mass of the piston and conrod as well as the mass of the counter weight predicted from the present study were indicated. If masses taking part on the both sides of the crankshaft were reduced as seen in Figure 14B, we may not expect a drastic variation in its dynamic equilibrium because of that the part cut off from the conrod behaves, more likely, as a part of crankshaft. As seen in Figure 14B, the counter weight is 250 g which is balancing the piston mass and 30% of the conrod mass. So, Figure 14B is a presentation of balancing of crankshaft according to the previous studies. The counterweight seen in Figure 14B is 250 g however; the one predicted via Equation (31) is 260 g. There is only 10 g difference between the present and former analyses which may generate at most 4% deviation.

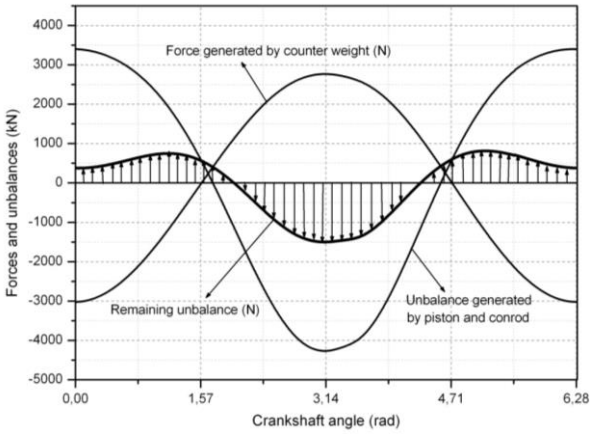

Figure 12. Vertical force and unbalances

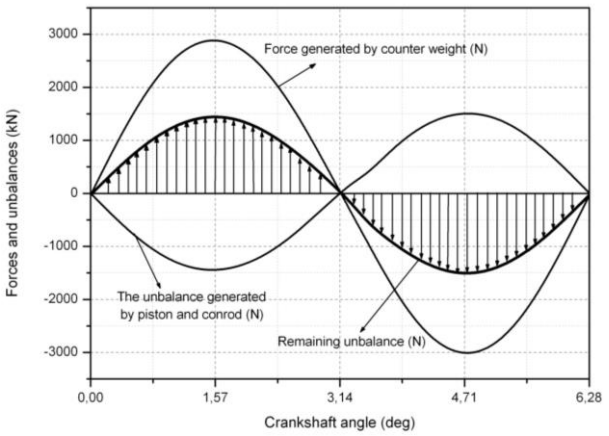

Figure 13. Horizontal force and unbalances

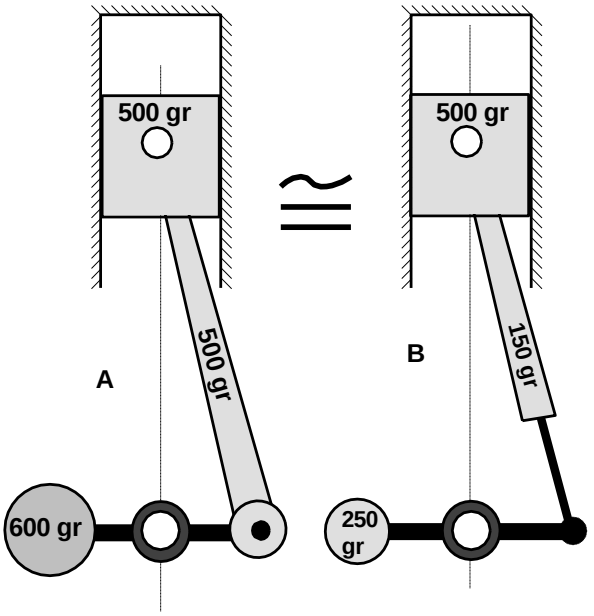

Figure 14. Conversion of counter weights determined with the present analysis and former analyses.

4. CONCLUSION

Via developing a thermodynamic-dynamic model the thermodynamic and dynamic behaviors of a single cylinder two-stroke gasoline engine has been investigated. The highest thermodynamic performance was obtained from the engine when the midpoint of the heat release interval was at 192° of crankshaft angle. The break torque of the analyzed engine was found to be about 45 Nm under the atmospheric charging conditions and 3000 rpm speed. The specific power of the engine was determined as 32 kW/liter. The thermodynamic values obtained from this analysis were found to be consistent with the result of previously conducted theoretical and experimental analyses. Analysis indicates that about 41% of the released heat is converted to the indicated work, 29% is transferred to the wall and 30% is taken away by the exhaust gases. Friction and pumping losses of the engine was predicted as about 10% of indicated work. While the intake air pressure was changing from 1 bar to 0.5 bar, the engine torque changed from 45.6 to 19.85 Nm at 3000 rpm engine speed. At 45 Nm load and 3000 rpm speed, the speed fluctuation of the engine was found to be about 3%. The difference of counter weights determined by former and present analyses was found to be less than 5%. The pressure rise ratio of the engine was estimated as $\frac{dp}{d\theta} \cong 2\ bar/\deg$ for the 192° heat release interval midpoint.

NOMENCLATURE

A_i instantaneous heat transfer area (m^2)
C a constant to quantify the released heat during the cycle (J/rad)
C_{km} torsional viscous damping coefficient at conrod bearing (Nms/rad)
C_s dimensionless friction coefficient at piston side surface
C_h torsional viscous damping coefficient at main bearing (Nms/rad)
C_p lateral viscous damping coefficient at piston surface (Ns/m)
F_w gas force exerting onto the piston (N)
F_{ch} crankcase pressure force (N)
F_{bx} x component of the conrod force exerting on piston (N)
F_{by} y component of the conrod force exerting on piston (N)
F_{dx} x component of the force generated by counter weight (N)
F_{dy} y component of the force generated by counter weight (N)
F_{kx} horizontal force applied by crankpin to conrod (N)
F_{ky} vertical force applied by crankpin to the conrod (N)
F_{zx} horizontal trust force exerting on engine block (N)
F_{zy} vertical trust force exerting on engine block (N)
F_∞ ring pack friction (N)
h cylinder heat transfer coefficient (W/m^2K)
h_p distance between piston top and gudgeon pin center (m)
I_{kr} crankshaft mass inertia moment (m^2kg)
I_b conrod mass inertia moment (m^2kg)
k specific heat at constant pressure/specific heat at constant volume
m mass of working gas (kg)
m_b mass of conrod (kg)
m_d mass of counter weight (kg)
m_p mass of piston (kg)
M_f moment generated by load-dependent friction at crankpin bearing (Nm)
M_τ moment generated by load-dependent frictions at main bearings (Nm)
M_s starter motor moment (Nm)
M_q External moment applied by the foundation to the engine (Nm)
n stroke counter

p pressure (Pa)
p_w gas pressure exerting on piston top (Pa)
p_{ch} gas force exerting on piston bottom (Pa)
p_{i-1} pressure corresponding to any θ_{i-1}
p_i pressure corresponding to θ_i
q heat per kg of air (J/kg)
Q_p heat released during the cycle (J)
q_p heat released per kg of air during the cycle (J/kg/cycle)
Q_w heat transferred to the wall during the cycle (J)
q_w heat transferred to the wall per kg of air during the cycle (J/kg/cycle)
R crank radius (m)
R_d radial distance of counter weight from the crankshaft center (m)
$\Re$ gas constant (J/Kg K)
T temperature (K)
T_w wall temperature (K)
t time (s)
u internal energy per kg of air (J/kg)
v specific volume of air (m^3/kg)
V volume of the gas (m^3)
V_{i-1} volume corresponding to θ_{i-1}
V_i volume corresponding to θ_i
V_p average velocity of the piston during a stroke (m/s)
W_i indicated work per cycle (J)
W_p pumping work per cycle (J)
W_f friction work per cycle (J)
W_b shaft work per cycle or brake work per cycle (J)
x coordinate element (m)
x_b conrod gravity center location in x (m)
y coordinate element (m)
y_p piston top location in y (m)
y_b conrod gravity center location in y (m)
θ angular position of the crankshaft respect to the initial position, Fig. 1, (rad)
$\dot{\theta}$ angular speed of the crankshaft (rad/s)
$\ddot{\theta}$ angular acceleration of the crankshaft (rad/s^2)
ω engine speed , $\dot{\theta}$, (rad/s)
Ω a dimensionless constant to quantify the heat release duration
ψ conrod angle with cylinder axis (rad)
φ a dimensionless constant to indicate the location of maximum heat release
λ conrod length (m)
λ_{cg} distance from conrod big end center to gravity center (m)
η_i indicated thermal efficiency
η_b brake thermal efficiency

REFERENCES

1. Blair G. P., "Design and Simulation of Two-Stroke Engines", **U.S.A: Society of Automotive Engineers, Inc.,** (1996)
2. Gabele P. A. and Pyle S. M., "Emissions from Two Outboard Engines Operating on Reformulated Gasoline Containing MTBE", **Environ. Science Technology,** 34: 368-372, (2000)
3. Amin M. A., Azhar A. A., MohdF. M. S., Zulkarnain A. L., "An experimental study on the influence of EGR rate and fuel octane number on the combustion characteristics of a CAI two-stroke cycle engine", ***Applied Thermal Engineering,*** 71: 248-258, (2014)
4. Pradeep V., Bakshi S., Ramesh A., "Scavenging port based injection strategies for an LPG fuelled two-stroke spark-ignition engine", ***Applied Thermal Engineering,*** 67: 80-88, (2014)
5. Volckens J., Olson D. A., Hays M. D., "Carbonaceous species emitted from hand held two-stroke engines", ***Energy Procedia***, 45: 739 – 748, (2014)
6. Cantore G., Mattarelli E., Rinaldini C.A., " A new design concept for 2-Stroke aircraft Diesel engines", ***Energy Procedia***, 45: 739–748, (2014)
7. Chehroudi B., Schuh D., "Intake-port flow behavior in a motored and fired two-stroke research engine", ***Experimental Thermal and Fluid Science,*** 10:86-100, (1995)
8. Semin N.M.I.N. Ibrahim Rosli A. Bakar and Abdul R. I., "In-cylinder flow through piston-port engines modeling using dynamic mesh", ***Journal of Applied Sciences Research***, 4(1): 58-64, (2008)
9. Li X., Zhang L., Fanga J., Huang Z., Xi H., " Combustion and emission characteristics of a two-stroke diesel engine operating on alcohol", ***Renewable Energy***, 30: 2075–2084, (2005)
10. Mattarelli E., Cantore G., and Rinaldini C.A., "Advances in the design of two-stroke, high speed, compression ignition engines", ***Advances in Internal Combustion Engines and Fuel Technologies,*** Chapter 5 DOI: 10.5772/54204, (2013)
11. Uyumaz A., Solmaz H., Yılmaz E., Yamık H., Polat S., "Experimental examination of the effects of military aviation fuel JP-8 and biodiesel fuel blends on the engine performance, exhaust emissions and combustion in a direct injection engine", ***Fuel Processing Technology***, 128: 158–165, (2014)

12. Ismail H.M., Ng H.K., Gan, S., Lucchini, T., "Computational study of biodiesel–diesel fuel blends on emission characteristics for a light-duty diesel engine using open FOAM", ***Applied Energy***, 111: 827–841, (2013)
13. Karabulut H., Ersoy H., "Dynamic Behaviors of a Two-Cylinder Four-Stroke Internal combustion Engine", ***Gazi University Journal of Science,*** 25(2):519-532, (2012)
14. Awrejcewicz J., Kudra G., "The piston-connecting rod-crankshaft system as a triple physical pendulum with impact", ***International Journal of Bifurcation and Chaos***, 15(7): 2207-2226, (2005)
15. Karabulut H., Öztürk E., Çinar C., "Tek silindirli bir dizel motorunun dinamik ve titreşim analizleri", ***Journal of the Faculty of Engineering and Architecture of Gazi University*** 27(3): 491-500, (2012)
16. Quintero H.F., Romero C. A., Useche L. V. V., "Thermodynamic and dynamic of an internal combustion engine with a noncircular-gear based modified crank-slider mechanism", ***12th IFToMM World Congress,*** *Besançon (France)* 1-6, (2007)
17. Tan Y-C, Ripin Z. M., "Technique to determine instantaneous piston skirt friction during piston slap", ***Tribology International,*** 74:145-153, (2014)
18. Tan Y. C., Ripin Z. M., " Analysis of Piston Secondary Motion", ***Journal of Sound and Vibration***, 332: 5162-5176, (2013)
19. Reis,V. L., Daniel G. B., Cavalca K. L., "Dynamic analysis of a lubricated planar slider–crank mechanism considering friction and Hertz contact effects", ***Mechanism and Machine Theory***, 74: 257–273, (2014)
20. Livanos G. A., Kyrtatos N. P., "Friction model of a marine diesel engine piston assembly". ***Tribology International***, 40: 1441–1453, (2007)
21. Rahnejat H., "Tribology and dynamics of engine and powertrain: fundamentals, applications and future trends", **New Delhi: Woodhead Publishing Limited**, (2010)
22. Perera, M. S. M., Theodossiades S. and Rahnejat H., "Elasto-multi-body dynamics of internal combustion engines with tribological conjunctions", ***Proc IMechE Part K: J Multi-Body Dynamics***, 224: 261–277, (2010)
23. Allmaier H., Sander D.E., Reich F.M., "Simulating friction power losses in automotive journal bearings", ***Procedia Engineering,*** 68: 49 – 55, (2013)
24. Hu, Y., Cheng, H.S., Arai, T., et al., "Numerical simulation of piston ring in mixed lubrication – a non-axisymmetrical analysis", ***Journal of Tribology***, 116: 470–478, (1994)
25. Bedajangam S. K., Jadhav N. P., "Friction losses between piston ring-liner assembly of internal combustion engine: a review", ***International Journal of Scientific and Research Publications***, 3(6):1-3, (2013)
26. Guzzomi A. L., Hesterman D. C., Stone B. J., "The effect of piston friction on engine block dynamics", ***Proc IMechE Part K: J Multi-Body Dynamics***, 221: 277–289, (2007).
27. Balakrishnan, S., Howell-Smith, S. and Rahnejat, H., "Investigation of reciprocating conformal contact of piston skirt-to-surface modified cylinder liner in piston skirt-to-surface modified cylinder liner", ***Proc IMechE Part C: Journal of Mechanical Engineering Science,*** 219(11): 1235-1247, (2005)
28. Croes J., Iqbal S., "Literature survey: bearing losses", **EC - 7th Framework Programme - Theme ICT,** (2009)
29. Bălan M. R. D., Stamate V. C., Houpert L., Olaru D. N., "The influence of the lubricant viscosity on the rolling friction torque", ***Tribology International***, 72:1–12. (2014)
30. Andersson S., Soderberg A., Bjorklund S., "Friction models for sliding dry, boundary and mixed lubricated contacts", ***Tribology International***, 40: 580–587, (2007)
31. Söndgen S., Predki W., "Power loss and axial load carrying capacity of radial cylindrical roller bearing", ***Power Transmission Engineering***, 42-47, (2013)
32. Karabulut H., "Dynamic model of a two-cylinder four-stroke internal combustion engine and vibration treatment", ***International Journal of Engine Research***, 0(0):1-12, (2012)
33. Metallidis P., Natsiavas S., "Linear and nonlinear dynamics of reciprocating engines", ***Internatioal Journal of Non-linear mechanics***, 38: 723-738, (2003)
34. Pasricha M. S., Hashim F. M., " Effects of the reciprocating mass of slider-crank mechanism on torsional vibration of diesel engine system", *Asean* ***Journal on Science and Technology for Development***, 23(1): 71-81, (2006)
35. Giakoumis E. G., Rakopoulos C. D., Dimaratos A. M., "Study of crankshaft torsional deformation under steady-state and transient operation of turbocharged diesel engines", ***Proc. IMechE Part K: J. Multi-body Dynamic,*** (222):17-30, (2008)
36. Spitsov O., "Heat transfer inside internal combustion engine: modeling and comparison with experimental data", ***Master Thesis; Lappeenranta University of Technology***, (2013)
37. SKF group, SKF rolling bearings catalogue, (2013)
38. Storakers B., Elaguine D., "Hertz contact at finite friction and arbitrary profiles", ***Journal of the Mechanics and Physics of Solids***, 53:1422–1447, (2005)
39. Mavropoulos G.C., "Experimental study of the interactions between long and short term unsteady heat transfer responses on the in-cylinder and exhaust manifold diesel engine surfaces", ***Applied Energy***, 88:867-881, (2011)
40. Yap D., Karlovsky J., Megaritis A., Wyszynski M. L., Xu H., "An investigation into propane homogeneous charge compression ignition (HCCI) engine operation with residual gas trapping", ***Fuel***, 84: 2372–2379, (2005)
41. Megaritis A., Yap D., Wyszynski M.L., "Effect of water blending on bioethanol HCCI combustion with forced induction and residual gas trapping", ***Energy***, 32:2396–2400, (2007)